Physics Letters B 773 (2017) 663–671

Contents lists available at ScienceDirect

Physics Letters B

www.elsevier.com/locate/physletb

Secondary scintillation yield of xenon with sub-percent levels of CO_2 additive for rare-event detection

The NEXT Collaboration

C.A.O. Henriques [a], E.D.C. Freitas [a], C.D.R. Azevedo [c], D. González-Díaz [i], R.D.P. Mano [a], M.R. Jorge [a], L.M.P. Fernandes [a], C.M.B. Monteiro [a,*], J.J. Gómez-Cadenas [b,1], V. Álvarez [b], J.M. Benlloch-Rodríguez [b], F.I.G.M. Borges [d], A. Botas [b], S. Cárcel [b], J.V. Carrión [b], S. Cebrían [e], C.A.N. Conde [d], J. Díaz [b], M. Diesburg [f], R. Esteve [g], R. Felkai [b], P. Ferrario [b], A.L. Ferreira [c], A. Goldschmidt [h], R.M. Gutiérrez [j], J. Hauptman [k], A.I. Hernandez [j], J.A. Hernando Morata [i], V. Herrero [g], B.J.P. Jones [l], L. Labarga [m], A. Laing [b], P. Lebrun [f], I. Liubarsky [b], N. López-March [b], M. Losada [j], J. Martín-Albo [b,2], G. Martínez-Lema [l], A. Martínez [b], A.D. McDonald [l], F. Monrabal [l], F.J. Mora [g], L.M. Moutinho [c], J. Muñoz Vidal [b], M. Musti [b], M. Nebot-Guinot [b], P. Novella [b], D.R. Nygren [l,1], B. Palmeiro [b], A. Para [f], J. Pérez [b], M. Querol [b], J. Renner [b], L. Ripoll [n], J. Rodríguez [b], L. Rogers [l], F.P. Santos [d], J.M.F. dos Santos [a], A. Simón [b], C. Sofka [o,3], M. Sorel [b], T. Stiegler [o], J.F. Toledo [g], J. Torrent [b], Z. Tsamalaidze [p], J.F.C.A. Veloso [c], R. Webb [o], J.T. White [o,4], N. Yahlali [b]

[a] *LIBPhys, Physics Department, University of Coimbra, Rua Larga, 3004-516 Coimbra, Portugal*
[b] *Instituto de Física Corpuscular (IFIC), CSIC & Universitat de València, Calle Catedrático José Beltrán, 2, 46980 Paterna, Valencia, Spain*
[c] *Institute of Nanostructures, Nanomodelling and Nanofabrication (i3N), Universidade de Aveiro, Campus de Santiago, 3810-193 Aveiro, Portugal*
[d] *LIP, Departamento de Física, Universidade de Coimbra, Rua Larga, 3004-516 Coimbra, Portugal*
[e] *Laboratorio de Física Nuclear y Astropartículas, Universidad de Zaragoza, Calle Pedro Cerbuna, 12, 50009 Zaragoza, Spain*
[f] *Fermi National Accelerator Laboratory, Batavia, IL 60510, USA*
[g] *Instituto de Instrumentación para Imagen Molecular (I3M), Universitat Politècnica de València, Camino de Vera, s/n, Edificio 8B, 46022 Valencia, Spain*
[h] *Lawrence Berkeley National Laboratory (LBNL), 1 Cyclotron Road, Berkeley, CA 94720, USA*
[i] *Instituto Gallego de Física de Altas Energías, Univ. de Santiago de Compostela, Campus sur, Rúa Xosé María Suárez Núñez, s/n, 15782 Santiago de Compostela, Spain*
[j] *Centro de Investigación en Ciencias Básicas y Aplicadas, Universidad Antonio Nariño, Sede Circunvalar, Carretera 3 Este No. 47 A-15, Bogotá, Colombia*
[k] *Department of Physics and Astronomy, Iowa State University, 12 Physics Hall, Ames, IA 50011-3160, USA*
[l] *Department of Physics, University of Texas at Arlington, Arlington, TX 76019, USA*
[m] *Departamento de Física Teórica, Universidad Autónoma de Madrid, Campus de Cantoblanco, 28049 Madrid, Spain*
[n] *Escola Politècnica Superior, Universitat de Girona, Av. Montilivi, s/n, 17071 Girona, Spain*
[o] *Department of Physics and Astronomy, Texas A&M University, College Station, TX 77843-4242, USA*
[p] *Joint Institute for Nuclear Research (JINR), Joliot-Curie 6, 141980 Dubna, Russia*

ARTICLE INFO

Article history:
Received 16 April 2017
Received in revised form 14 August 2017
Accepted 7 September 2017
Available online 12 September 2017
Editor: W. Haxton

ABSTRACT

Xe–CO_2 mixtures are important alternatives to pure xenon in Time Projection Chambers (TPC) based on secondary scintillation (electroluminescence) signal amplification with applications in the important field of rare event detection such as directional dark matter, double electron capture and double beta decay detection. The addition of CO_2 to pure xenon at the level of 0.05–0.1% can reduce significantly the scale of electron diffusion from 10 mm/$\sqrt{\text{m}}$ to 2.5 mm/$\sqrt{\text{m}}$, with high impact on the discrimination

* Corresponding author.
E-mail address: cristina@gian.fis.uc.pt (C.M.B. Monteiro).
[1] NEXT Co-spokesperson.
[2] Now at University of Oxford, United Kingdom.
[3] Now at University of Texas at Austin, USA.
[4] Deceased.

http://dx.doi.org/10.1016/j.physletb.2017.09.017

Keywords:
Double beta decay
Neutrino
Rare event detection
Electroluminescence
Secondary scintillation
Xenon

efficiency of the events through pattern recognition of the topology of primary ionization trails. We have measured the electroluminescence (EL) yield of Xe–CO_2 mixtures, with sub-percent CO_2 concentrations. We demonstrate that the EL production is still high in these mixtures, 70% and 35% relative to that produced in pure xenon, for CO_2 concentrations around 0.05% and 0.1%, respectively. The contribution of the statistical fluctuations in EL production to the energy resolution increases with increasing CO_2 concentration, being smaller than the contribution of the Fano factor for concentrations below 0.1% CO_2.

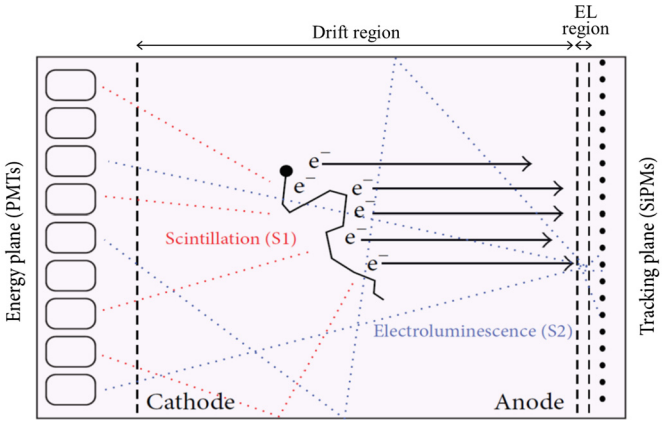

Fig. 1. Schematic of the EL-based TPC developed by the NEXT Collaboration for double-beta decay searches in ^{136}Xe.

1. Introduction

Many experiments aiming for rare event detection such as double beta decay (DBD) and double electron capture (DEC), with or without neutrino emission, as well as directional dark matter (DDM) use high-pressure xenon (HPXe) as the detection/target medium [1–7]. The physics behind these experiments is of paramount importance in contemporary particle physics and cosmology.

When compared to liquid xenon and double phase xenon TPCs [8–14], detection in the gas phase offers some important advantages. While the event detection in liquid TPCs allows for compactness and self-shielding, some features may be essential for the above experiments to succeed. The impact of background depends strongly on the achieved energy resolution, which is much better for event detection in gas than in liquid. Furthermore, event interaction in the gas will allow for discrimination of the rare event topological signature, as demonstrated for DBD and DEC detection [15,16,5], in contrast to the interaction in liquid, where the extremely reduced dimensions of the primary ionization trail rules out any possible trail pattern recognition.

In particular, optical TPCs based on secondary scintillation (electroluminescence) amplification of the primary ionization signal are the most competitive alternatives to those based on charge avalanche amplification. For the latter, the limited charge amplification at high pressure impacts the energy resolution, yielding at present a best value around 3% at 2.5 MeV for a 1 kg-scale prototype based on micromegas [17], to be compared to 0.7% obtained for an electroluminescence (EL) amplification prototype of similar dimensions [18]. In addition, when compared to conventional electronic readout of the charge avalanche, EL optical readout through a photosensor has the advantage of mechanically and electrically decoupling the amplification region, rendering more immunity to electronic noise, radiofrequency pickup and high voltage issues.

Fig. 1 depicts a schematic of a typical optical TPC. Most of the gas volume is occupied by the conversion/drift region where the radiation interaction takes place exciting or ionizing the gas atoms/molecules and leading to the emission of primary scintillation (the t_0 signal of the event) resulting from the gas de-excitation or electron/ion recombination. A low electric field, below the gas excitation threshold, is applied to the drift region to minimize recombination and to guide the primary electrons towards a shallow region with electric field intensity between the gas excitation and ionization thresholds, the scintillation region. Upon crossing this region, each electron gains from the electric field enough kinetic energy to excite the gas atoms/molecules by electron impact, leading to a large scintillation output upon gas de-excitation (electroluminescence). A pixelated photosensor plane enables to determine the x- and y-positions of the primary electrons arriving at the EL region, and the time interval between primary and EL scintillation pulses enables to determine the z-position of where the ionization takes place.

Absolute values of the EL light yield have been measured in uniform electric fields [19–21] and in the modern micropatterned electron multipliers, as GEM, THGEM, MHSP and micromegas [22–24]. The statistical fluctuations in the EL produced in charge avalanches are dominated by the statistical fluctuations in the total number of electrons produced in the avalanche, since all the electrons contribute to EL production. On the other hand, the statistical fluctuations in the EL produced for uniform electric fields below the gas ionization threshold are negligible when compared to those associated with the primary ionization formation [25]. The latter situation is most important when event to background discrimination is also based on the energy deposited in the gas, as is the case of DEC and neutrinoless double beta decay, where the best achievable detector energy resolution is important for efficient background rejection.

The effectiveness of event discrimination based on the topological signature of the ionization trail is related to the low electron drift velocity of xenon and, mainly, to its large electron diffusion. The large electron diffusion is determined by the inefficient electron energy loss in elastic collisions with the xenon atoms, in particular in the range of reduced electric fields of few tens of V/cm/bar used in the drift region. Diffusion hinders the finer details of the ionization trail, especially for large drift distances, and the discrimination based on the topological signature of the events becomes less effective [26].

The aforementioned problem can be mitigated by adding a molecular gas, like CO_2, CH_4 or CF_4, to pure xenon. With the addition of such molecules, new molecular degrees of freedom from vibrational and rotational states are made available for electron energy transfer in inelastic collisions. In this case, the energy distribution of the ionization electron cloud in the drift region tends to build up around the energy of the first vibrational level, typically at ∼0.1 eV, even in the presence of minute concentrations of molecular additives.

Until recently, it was believed that the presence of molecular species in the noble gas would dramatically reduce the EL yield that could be achieved. Experimental studies performed for Ar [27] have shown that the presence of CO_2 and CH_4 in concentrations

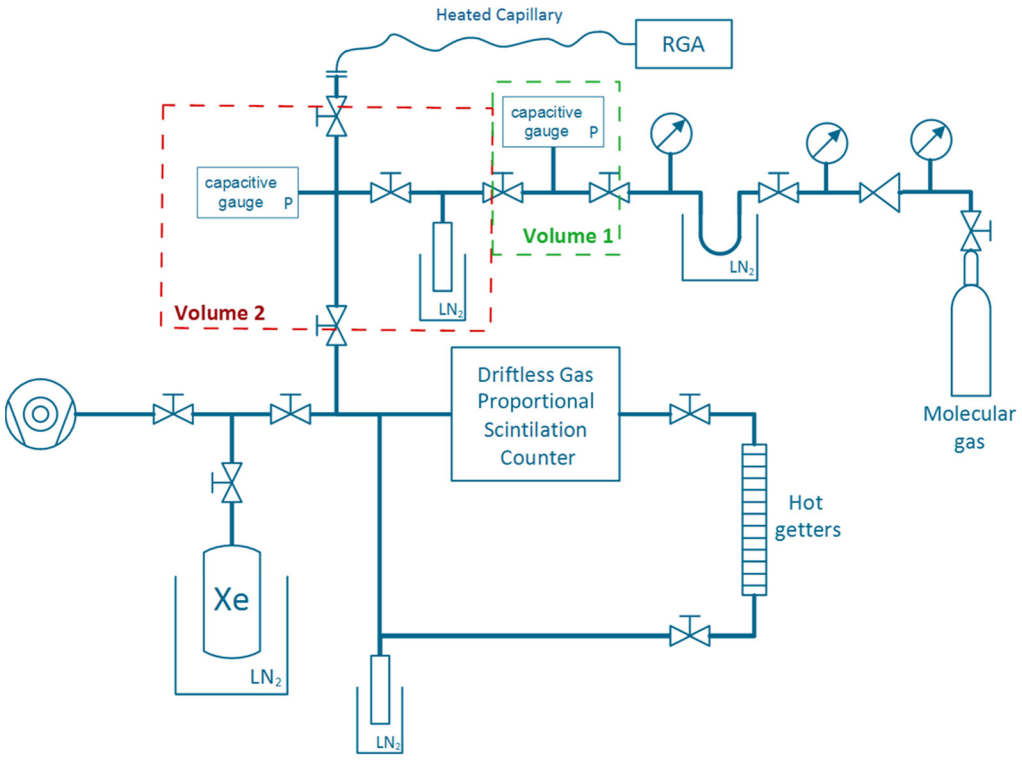

Fig. 2. Schematic of the experimental apparatus, including the gas proportional scintillation counter, the gas circulation and purifying system with SAES St-707 getters, the gas entrance and exit systems including the turbo-pump, two calibration volumes (volume 1 in green, volume 2 in red), the liquid nitrogen mixing vessels and the RGA connection through a heated capillary. (For interpretation of the references to colour in this figure legend, the reader is referred to the web version of this article.)

as low as ∼50 ppm and ∼200 ppm, respectively, resulted in an EL reduction above 70%. Detailed Monte Carlo simulation studies of electron drift in xenon at atmospheric pressure and room temperature [28] have shown that the average number of elastic collisions between successive inelastic collisions is very large, of the order of 10^4, for the typical reduced electric fields applied to the EL region. This fact partly explained the importance of gas purity for the EL yield of noble gases: if an electron has significant probability of colliding with a molecular impurity before it obtains from the electric field sufficient energy to excite a noble gas atom, it may lose part of its energy without leading to EL photon emission, resulting in a decrease in the EL production. Depending on the conditions, excimer quenching, photo-absorption and dissociative attachment can jeopardize performance as well.

Within the NEXT Collaboration [1], which has built a HPXe TPC for DBD studies with the ^{136}Xe isotope, we proposed to revisit the addition of molecular additives to xenon, at sub-percent level, to reduce electron diffusion in the TPC, hence improving the topological discrimination capabilities. Preliminary experimental studies and simulations for different concentrations of CO_2 and CH_4 gases that are common in TPCs and whose elementary cross-sections are well known, have shown encouraging results [29], leading to acceptable EL losses and only small degradation in the detector energy resolution. Simulation results obtained with Magboltz [38] have shown that Xe–CO_2 mixtures with concentrations of 0.05–0.1% of CO_2 would be sufficient to reduce the transversal and longitudinal diffusion coefficients to acceptable values (~ 2.5 mm/$\sqrt{\text{m}}$). These concentrations are almost one order of magnitude lower than those needed for CH_4, in order to obtain a similar diffusion reduction [29].

Those results led us to perform a detailed study on the effect of the addition of CO_2 to pure xenon both on the EL yield and on the energy resolution, for additive concentrations below 1% [29]. In this work we present those studies. CO_2 is a priori the most interesting option due to its low cost and easy handling, since it is non-flammable.

2. Experimental setup and methodology

The experimental setup especially projected for these studies includes a Gas Proportional Scintillation Counter (GPSC) [25], which is connected to a gas re-circulation system in order to continuously purify the gas or the mixture using SAES St-707 getters; a Residual Gas Analyser (RGA) that provides a real-time direct measurement of the molecular additive concentrations; a vacuum pumping system to maintain the RGA in continuous operation; associated electronics and suitable control and data-acquisition electronics for both systems, the RGA and the GPSC. The xenon gas is 4.8 grade from Messer containing less than 1 ppm of the main molecular gasses. The getter efficiency is very effective in removing the outgassing from the detector; the EL degradation is very slow after closing the gas circulation through the getters while presenting a much faster recovery when the gas circulation is restored. E.g., it takes two hours for the EL to be reduced by 20% after closing the getters, while it takes only 10 minutes to restore the original performance after gas circulation through the getters is resumed. Therefore, xenon purity in normal detector operation is similar or even better than that of the gas inside the original bottle. The main components of the experimental setup are illustrated in Fig. 2.

The GPSC used in this work is depicted in Fig. 3. It is of the 'driftless' type, i.e. without drift region, and has been already used in [30,31]. This design was chosen for the present work because it allows to study the influence of molecular additives on the EL parameters, minimizing the effects that may arise in the electron drift through the drift region and gas scintillation transparency.

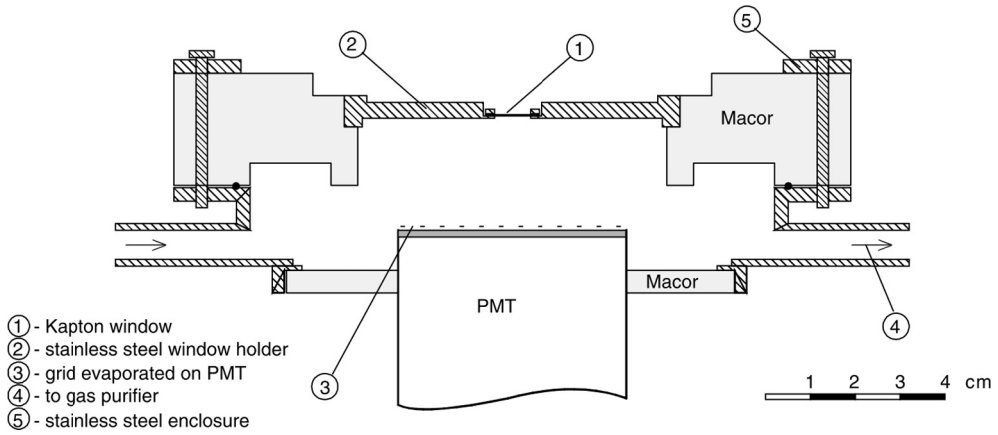

Fig. 3. Schematic of the driftless GPSC used in this work, including its principal components.

The EL region, 2.5 cm long, is delimited by a Kapton radiation window (8 mm in diameter, mounted on a stainless steel holder) aluminised on the inner side, and by the PMT quartz window, vacuum-evaporated with a chromium grid (100 μm width and 1000 μm spacing), electrically connected to the photocathode pin of the PMT. The EL electric field is established by applying a negative high voltage to the detector window and its holder (4 to 10.5 kV), which are insulated from the stainless steel detector body by a ceramic material (Macor), being the detector body, the chromium grid of the PMT window and its photocathode kept at 0 V. More information on this detector can be found in [30,31]. The reduced electric field inside the detector is set below the gas ionization threshold in order for EL to be produced without any charge multiplication in the EL region.

A 2-mm collimated, 5.9 keV x-ray beam from a ^{55}Fe radioactive source irradiated the detector window along the detector axis, being the 6.4-keV x-rays of the Mn K_β line absorbed by a chromium film. The 5.9 keV x-rays interact in the gas resulting in the release of electrons and photons. These ionization electrons are accelerated throughout the EL region exciting the noble gas atoms and inducing EL as a result of the atoms' de-excitation processes. The amount of EL is more than 3 orders of magnitude higher than primary scintillation. The EL pulse is collected by the PMT, whose output signal is subsequently shaped, amplified and, finally, digitized through a Multi-Channel Analyser (MCA). A typical pulse-height distribution obtained in the MCA for 5.9 keV x-rays is depicted in Fig. 4a.

In a driftless chamber, the amount of EL depends on the distance travelled by the primary electron cloud in the EL region and, therefore, on the x-ray interaction depth. Consequently, the pulse-height distribution generated by the MCA has the typical Gaussian shape (from a monoenergetic line) convoluted with an exponential tail towards the low-energy region, due to the exponential law of the x-ray attenuation. Since, for 5.9-keV x-rays, the absorption length in 1 bar of xenon is about 2.7 mm, very small when compared to the long EL region of 25 mm, the observed full absorption peak in the pulse-height distribution has an almost Gaussian-like shape.

The intrinsic response of the GPSC for 5.9 keV x-rays was obtained by deconvolution of the overall full absorption peak distribution into a sum of a large number, 250, of Gaussian functions corresponding to x-ray interactions at successive depths, $\Delta z = 0.01$ cm, with areas decreasing according to the exponential absorption law for the 5.9 keV x-rays and with the same relative FWHM, which was left as a free parameter. The centroid of each Gaussian follows the integration of the solid angle subtended by the PMT photocathode along the path corresponding to each x-ray penetration, being the centroid of the rightmost Gaussian, i.e. the one having the highest centroid, left as a free parameter. Fig. 4b depicts an experimental pulse-height distribution for the full energy peak and the resulting fit obtained by the deconvolution procedure used, denoting a very good agreement. The GPSC pulse amplitude and energy resolution were taken from the centroid and FWHM of the Gaussian corresponding to x-ray interactions taking place just below the window, i.e. the rightmost one. The obtained amplitude is within 2% of the peak channel of the full energy peak, Fig. 4b. The obtained energy resolution is somewhat below 7%, instead of the ∼8% obtained for a Gaussian fit to the right side. Directly analysing the PMT pulse waveforms with a given duration (i.e. corresponding to the same x-ray penetration) we obtained a Gaussian shape pulse-height distribution with energy resolution not higher than 7.3%, absolute value. The "true" energy resolution should be lower than this value, since the signal-to-noise ratio in this case is not negligible, contributing to higher statistical fluctuations.

The small volumes in Fig. 2, each one read by an accurate capacitive pressure gauge, were used to calibrate the RGA. Volume 2 is filled with pure xenon from the detector volume, while volume 1 is filled with CO_2. For the RGA calibration, only these volumes were used, being isolated from the detector volume before the reference mixtures were done avoiding, in this way, any error that might result from CO_2 adsorption to the inner surfaces of the GPSC and, mainly, to the getters. We consider that the amount of CO_2 adsorbed or released by the walls of the calibration volumes is negligible. The calibration process has shown a good linear correlation between the concentration measured in the RGA and the initial additive concentration based on the pressure gauge readings, within the studied concentration range. In order to avoid a pressure-dependent non-linearity of the RGA, calibration and detector operation have been carried out at the same total pressure of about 1.13 bar, for both pure xenon and its mixtures.

The EL studies were performed when the RGA partial pressures stabilized and, likewise, the additive concentration was calculated from an average over several measurements done during the time interval when the EL studies were performed.

Before setting each mixture, a measurement of the CO_2 background was performed in the GPSC filled with pure xenon, having the getters at 250 °C, in order to ensure maximum xenon purity. This background was, afterwards, subtracted from the RGA CO_2 reading once the mixture was done. For CO_2 only mass 44 peak was used, as the other peaks are superimposed on other molecular species, while for Xe all the peaks are considered.

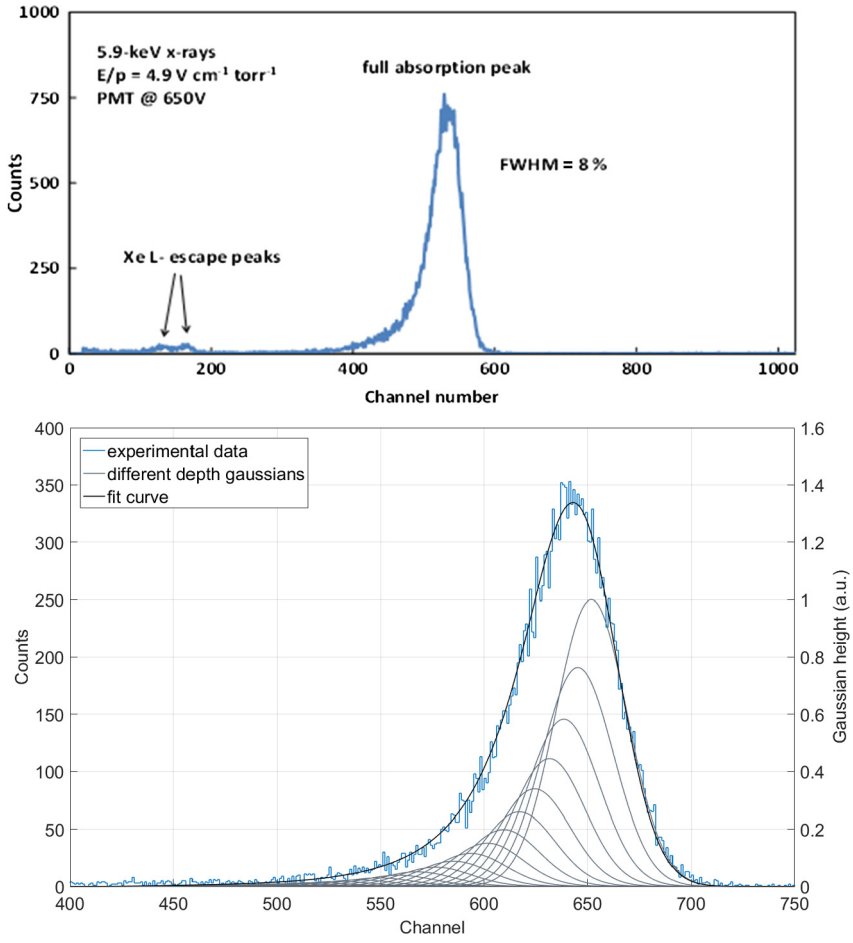

Fig. 4. a) Pulse-height distribution for 5.9-keV x-rays absorbed in the xenon driftless GPSC for a reduced electric field of 3.7 kV/cm/bar; b) detail of the full energy peak (blue histogram), the fit function (black solid line), and some of the Gaussians resulting from the deconvolution procedure used in this work (black and grey solid lines). (For interpretation of the references to colour in this figure legend, the reader is referred to the web version of this article.)

As the hot getters react with CO_2, the getter temperature was reduced to 80 °C before the mixture was done. At this getter temperature CO_2 is only slightly absorbed. On the other hand, the EL parameters in pure xenon were found to degrade only slightly and only after several days of operation when cooling down the getters from 250 °C to 80 °C. Furthermore, it was observed that, despite the CO_2 being absorbed in the getters, part of it is also transformed into CO that escapes to the gas phase, as observed by the correlated growth of the partial pressure at mass 28 (related with CO) as the concentration of CO_2 decreases. This effect increases with increasing getter temperature. Therefore, some CO is present in the Xe–CO_2 mixtures, with concentrations that are roughly constant for all the studied mixtures, for a getter operation temperature of 80 °C. Simulations have shown that the impact of the presence of CO on the yield is small, within a 10% effect at most, for the lowest CO_2 concentrations. The simulations were carried out using the same algorithms as in [29] and considering CO concentrations below 0.05%.

In this work only relative values were measured for the EL yield. Absolute values for the EL reduced yield, Y/N, N being the density of the molecules in the gas, were obtained normalizing the relative pulse amplitude as a function of reduced electric field, E/N, obtained in this work for pure xenon, to the absolute values of the EL reduced yield obtained in [19]. The same normalization constant was, then, used to normalize the remaining EL curves obtained for the different mixtures.

3. Experimental results

In Fig. 5, the reduced EL yield, number of photons produced per electron per cm of path divided by the atomic number density, Y/N, as a function of the reduced electric field, E/N, applied to the EL region[5] is shown for different CO_2 concentrations added to pure xenon. The two data sets for the 0.174% of CO_2 are related to two independent measurements. Interestingly, the reduced yield exhibits the typical approximate linear dependence of EL with reduced electric field even in the presence of CO_2. The solid lines present fits to the data, excluding the data points near the EL threshold where the EL response of GPSCs deviates from the linear trend [30]. As expected, the EL yield decreases as the CO_2 amount increases. Nevertheless, CO_2 concentrations of ∼0.05%, which allow an overall electron diffusion around 2.5 mm/$\sqrt{\text{m}}$ [29], can be acceptable in terms of EL yield since, in spite of having an EL yield reduction up to 35% when compared to pure xenon, this reduction may be tolerable in the cases where the EL is large enough. For comparison, it must be recalled that such a reduction is achieved in Ar mixtures when CO_2 concentration reaches 10 ppm [27].

As anticipated, for the same reduced electric field intensity, the EL threshold increases with increasing CO_2 content since, upon

[5] At $T = 293$ K we have Y/N (ph/e/atom $\times 10^{-17}$ cm^2) $= 2.276 \times 10^3 Y/p$ (ph/e cm^{-1} bar^{-1}) and E/N (Td) $= 2.276 E/p$ (kV cm^{-1} bar^{-1}); (1 Townsend $= 10^{-17}$ V cm^2).

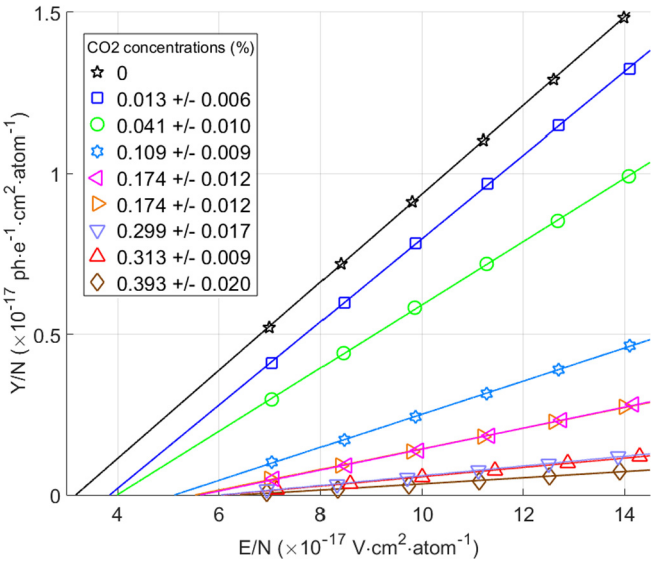

Fig. 5. EL reduced yield, Y/N, as a function of the reduced electric field, E/N, for different concentrations of CO_2 added to pure xenon. The errors are less than few percent and, hence, the error bars are within the symbols. The solid lines are linear fits to the data.

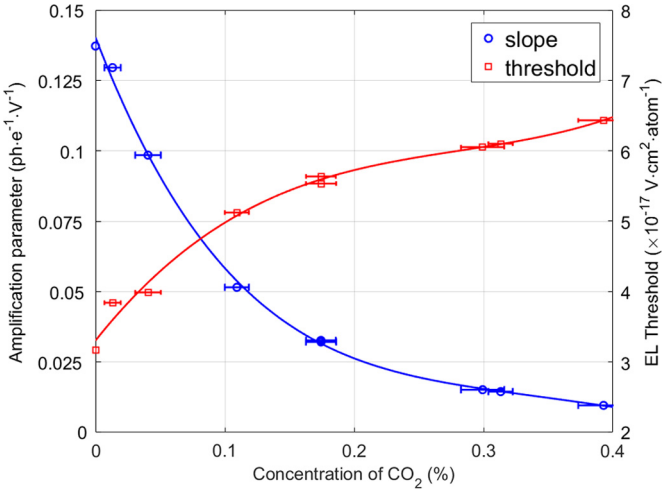

Fig. 6. Light amplification parameter and EL threshold of the lines fitted to the reduced EL yield (Fig. 5). The solid lines serve only to guide the eye.

colliding with a CO_2 molecule, the electron loses energy to rotational and vibrational excited states, reducing the average electron energy. Although qualitative in nature, the behaviour of the EL threshold shows how this cooling seems to be very efficient up to concentrations around 0.1% (as indicated by Magboltz simulations), values for which the EL loss remains acceptable, hinting that a compromise in terms of electron cooling/excimer scintillation does exist. Additional losses can be expected in CO_2 from dissociative attachment and excimer quenching, this last one being indeed the main source identified earlier in [27]. Fig. 6 summarizes the EL threshold and reduced yield slope, from Fig. 5 data, as a function of CO_2 concentration.

The impact of the molecular additive on the TPC energy resolution is an important parameter to be considered, in particular in double electron capture and in neutrinoless double beta decay detection, as it is a tool to effectively discriminate the rare events against background. In Fig. 7 we present the GPSC energy resolution (FWHM) for 5.9 keV x-rays as a function of reduced electric field, for the different CO_2 concentrations used in this work. The

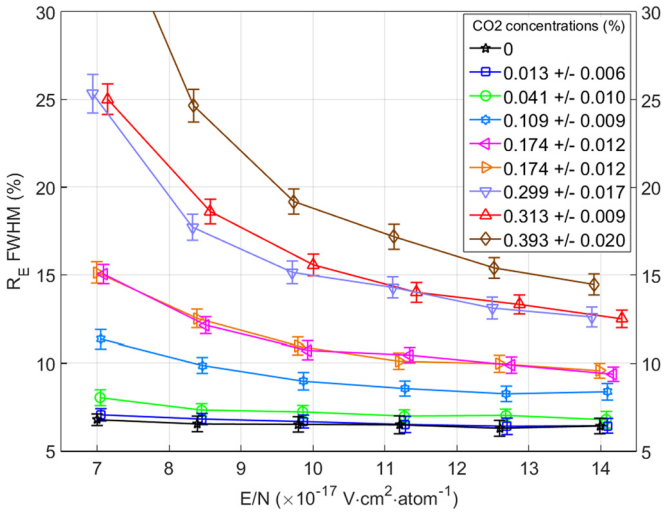

Fig. 7. Detector energy resolution as a function of E/N for 5.9 keV x-rays and for different concentrations of CO_2. The solid lines serve only to guide the eye. Error bars include both statistical and estimated systematic errors.

error bars include the uncertainties in the fit and the statistical error associated to multiple readings, added quadratically. The errors are overestimated as we do not know the correlation between both values. Nevertheless, we assumed these conservative errors.

From the experimental data, centroid and FWHM, it is possible to assess the fluctuations in the EL production assuming that the obtained pulse-height distributions are well-described by the mathematical model already discussed in the literature. The energy resolution (FWHM) of a GPSC, R_E, is given by [25]:

$$R_E = 2\sqrt{2\ln 2}\sqrt{\frac{\sigma_e^2}{\overline{N}_e^2} + \frac{1}{\overline{N}_e}\left(\frac{\sigma_{EL}^2}{\overline{N}_{EL}^2}\right) + \frac{\sigma_{pe}^2}{\overline{N}_{pe}^2} + \frac{1}{\overline{N}_{pe}}\left(\frac{\sigma_q^2}{\overline{G}_q^2}\right)} \quad (1)$$

where the first term under the square root describes the relative fluctuations in the number of ionization electrons induced by the interaction, N_e, the second term describes the relative fluctuations associated to the number of EL photons produced in the EL region per primary electron, N_{EL}, and the last two terms describe the relative fluctuations in the photosensor, namely the relative fluctuations in the number of photoelectrons released from the PMT photocathode by the EL burst, N_{pe}, and the relative fluctuations in the number of electrons collected in the PMT anode per photoelectron, i.e. the relative fluctuations in the gain of the electron avalanche in the PMT. The electronic noise is not included in Eq. (1) since it is negligible, as shown by the amplifier pulse waveforms in the oscilloscope. Since the process of photoelectron release from a photocathode by the incoming photons is described by a Poisson distribution, its variance is $\sigma_{pe}^2 = \overline{N}_{pe}$ and the relative fluctuations in the PMT are given by:

$$\frac{1 + \left(\frac{\sigma_q^2}{\overline{G}_q^2}\right)}{c\overline{N}_e\overline{N}_{EL}} = \frac{k}{\overline{N}_{EL}}, \quad (2)$$

c represents the light collection efficiency, related to the anode grid transparency (Fig. 3), 81%, to the PMT quantum efficiency, 20% for 172 nm, and to the average solid angle subtended by the PMT photocathode relative to the primary electron path in the EL region, 30%. Therefore, k is a constant, which depends on the scintillation readout geometry and on the photosensor itself (for our PMT we measured a relative gain fluctuation of 0.55).

From the data for pure xenon, we can experimentally determine the contributions to the energy resolution from the statistical

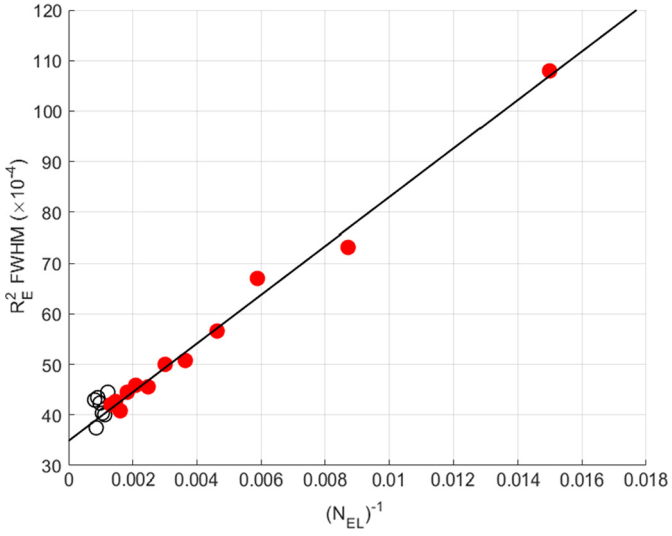

Fig. 8. The square of the energy resolution (R_E) as a function of the inverse of the average number of photons produced in the EL region per primary electron for 5.9 keV x-rays and for pure xenon. The solid line presents a linear fit to the data points in red. (For interpretation of the references to colour in this figure legend, the reader is referred to the web version of this article.)

fluctuations due to the primary ionization formation and due to the photosensor, since the contribution from the statistical fluctuations to the EL is negligible when compared to the other factors [25]. In Fig. 8 we depict R_E^2 as a function of N_{EL}^{-1} for pure xenon. A linear function, as imposed by Eq. (1), is fitted to the data points, excluding those with the highest N_{EL}, which depart from the linear trend. This behaviour is similar to the one observed in standard type GPSCs, with drift region [32,33]. The first term is obtained from the line interception with the vertical axis while $8\ln(2)k$ is the slope of the line. From Fig. 8 we obtain a Fano factor $F = \sigma_e^2/\overline{N}_e = 0.17 \pm 0.04$ for xenon, using a w-value of 22 eV [34], i.e. the average energy needed to produce one electron–ion pair in xenon ($N_e = E_x/w$, E_x being the x-ray energy; for x-rays the w-value does not depend on the applied electric field, above ~20 V/cm/bar, since recombination in this case is negligible). This result is in good agreement with the values normally found in the literature, between 0.13 and 0.25 [32,35–37]. In addition, the result we obtain for c from Eq. (2) (0.056) is similar to what is obtained from calculations based on the geometry (0.048). These agreements show the robustness of the present method.

The terms of Eq. (1) obtained from the fit in Fig. 8 (the 1st and the last 2), for the relative fluctuations in the primary ionization formation and for the relative fluctuations in the photosensor, are constant for all CO_2 concentrations studied in this work, since the Fano factor and the w-values of those mixtures are not expected to change significantly for these low additive concentrations, as shown by Degrad simulation [38], and k is constant for a given geometry and photosensor setup. Therefore, it is possible to determine the fluctuations associated to the EL production as a function of reduced electric field for the different mixtures, using the R_E data from Fig. 7, as these fluctuations are the only unknown variable in Eq. (1).

In Fig. 9 we present the square of the relative standard deviation in the number of EL photons produced in the EL region per primary electron,

$$Q = \left(\frac{\sigma_{EL}^2}{\overline{N}_{EL}^2}\right), \tag{3}$$

as a function of reduced electric field in the EL region, for the different concentrations of CO_2 added to pure xenon. A striking observation that can be made in Fig. 9 is that Q becomes non-negligible as the CO_2 concentration increases, largely independent of the reduced electric field. For a CO_2 concentration as low as 0.1% $Q \sim 0.08$, i.e. about half the value of the Fano factor, while for 0.2% CO_2 Q becomes comparable. For a CO_2 concentration of 0.05% Q is found to be around 0.02, a value that has a negligible impact on the energy resolution. For higher CO_2 concentrations and lower E/N, the signal-to-noise ratio decreases significantly, resulting in an artificially high energy resolution and, consequently, an over-estimated Q value obtained from Eq. (1), as the noise is not included in this equation. For that reason, those points are not included in Fig. 9. As the uncertainty in Q is dominated by the uncertainty in the energy resolution, the error bars are also over-estimated, as explained before.

The rise in the contribution from Q cannot be explained if we take only into account the effect of EL reduction with increasing CO_2, since even a reduction of one order of magnitude in EL still means a very high number of EL photons and, in addition, one would expect a decrease in Q with increasing electric field in the EL region, instead of an almost constant trend. We believe that this effect is due to dissociative electron attachment to

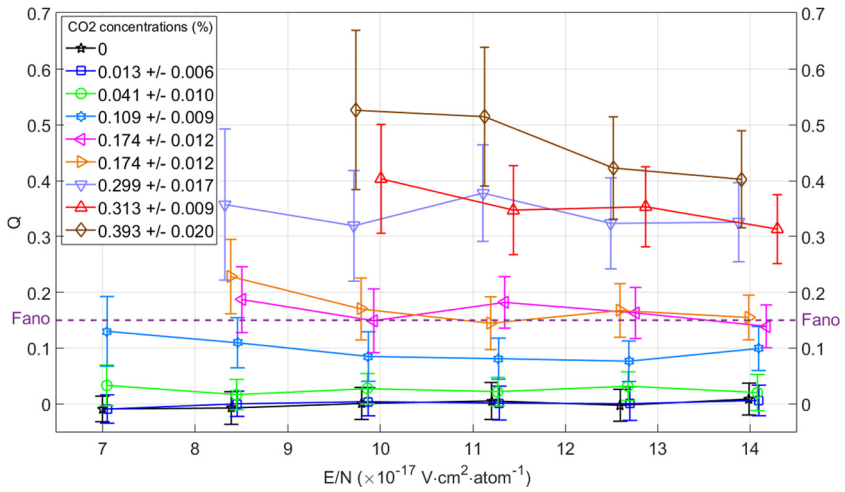

Fig. 9. Relative standard deviation in the number of EL photons per primary electron once squared (Q), as a function of the reduced electric field in the EL region (E/N) for different concentrations of CO_2. The solid lines serve only to guide the eye.

CO_2 molecules, for which we find a good quantitative agreement with simulations [39]; in the absence of this effect, simulations predict values for the Q-factor around 0.02, little dependent on concentration. Indeed, the cross-section for electron attachment is non-negligible and has narrow peaks for electron energies between 4–5 and 7–9 eV, e.g. see Fig. 1 in [40], and these are energies that the electrons will eventually reach in the EL region in order to be able to excite the xenon atoms. The simulated attachment implies for the highest CO_2 concentration a relatively modest 10's of %-level loss of ionization electrons; this effect is, therefore, not the only responsible for the EL reduction. For example, for the highest concentrations of CO_2, the electron attachment probability is about 65%, according to Magboltz simulation [41], which would lead to a maximum EL reduction of 65% if all attachment would happen right at the beginning of the electron path; however, experimental results show EL reductions above 90%. Most of the remaining EL reduction is explained by quenching. The presence of attachment becomes, nonetheless, the main source of fluctuations in the EL signal for concentrations already above 0.17% CO_2.

4. Discussion

CO_2 concentrations in the range of 0.05%–0.1% correspond to a characteristic size of the electron diffusion ellipsoid of $\sqrt[3]{\sigma_x\sigma_y\sigma_z} \cong 2.5\ \text{mm} \times \sqrt{\frac{10\ \text{bar}}{P}}$ after a 1 m drift through the TPC [29,39]. This value can be found for reduced drift fields in the range of $E/P =$ [20–30] V/cm/bar, by resorting to the latest Magboltz cross-section database. The drastic change experimentally observed in the EL threshold (Fig. 6) suggests that electron cooling is in fact strongly active even for these minute concentrations. Moreover, simulations indicate that a minimum of diffusion exists in the above field range; therefore, there is little to be gained by increasing (or decreasing) the drift field in the TPC. The presence of such minima can be found experimentally and theoretically for xenon mixtures and additives like CH_4 or TMA in [17], and it becomes narrower at low concentrations.

In pure xenon at 10 bar, electric fields in the aforementioned range pose no problems concerning charge recombination for primary electrons, as can be readily noticed, for instance, in [24]. For admixtures, however, the situation at high pressures is less clear. Some qualitative arguments can be drawn: in xenon at 5 bar and in a 0.22% TMA admixture, for example, the additional contribution to the Fano factor stemming from fluctuations in the charge recombination process is less than 0.1 [42]. Since the measured diffusion and drift coefficients are, in that case, similar to those simulated for the CO_2 optimum (0.05%–0.1%), and being the ionization density close to the one attempted in NEXT (10 bar), measurements performed in Xe–TMA can be used to estimate an upper bound to the effect expected in Xe–CO_2. Besides this initial charge recombination, it must be noted that the drift velocity will be reduced for optimum CO_2 concentrations by a factor of around 2, which is not expected to have a dramatic effect on the electron lifetime, according to the measurements performed in [17], again for TMA admixtures.

The above aspects will soon be evaluated for high pressures in NEXT-DEMO, a large prototype with a drift length of 30 cm and a hexagonal cross section of 8-cm apothem, operated with ∼1.5 kg of natural xenon at a pressure of 10 bar [43]. Other relevant effects like the pressure-dependence of the EL yields and the light fluctuations will also be evaluated. Simulations performed in [39] indicate that, despite the anticipated deterioration at high pressure, both the Q factor and the finite-statistic term from the PMTs can be kept at the level of the Fano factor at 10 bar, as long as the CO_2 concentration remains in the range of 0.05–0.1%. Concerning the primary scintillation yields, a tolerable reduction within a factor of 5–10 is expected in the same concentration range.

A possible drawback that can arise from the use of CO_2 is related to the gas stability in the long term and the associated formation of CO. This can be handled using specific getters for CO_2. On the other hand, being these devices cold getters, one has to evaluate the radon emanation.

5. Conclusions

We have performed experimental studies on the reduced electroluminescence yield of Xe–CO_2 mixtures at room temperature. We have demonstrated that the addition of CO_2 to pure xenon, at concentration levels of few tenths of a percent, does not kill the proportional electroluminescence (EL) yield entirely, as it has been assumed during the last decades. CO_2 concentrations of 0.05% and 0.1% at around atmospheric pressure lead only to an EL reduction of 35% and 70%, respectively, relative to that produced in pure xenon at the same reduced electric field. Such a modest reduction seems tolerable, provided the number of photons produced per ionization electron is very large and also because it may be readily compensated by increasing the reduced electric field, since higher field can be applied to the EL region, as the ionization threshold increases with increasing CO_2 concentration.

On the other hand, the intrinsic energy resolution of xenon-based TPCs (i.e., photo-detection statistics neglected) degrades with increasing CO_2 concentration; for a concentration of 0.05% the contribution of the statistical fluctuations associated to EL production is a factor of 6 lower than the Fano factor, for 0.1% nearly half and for 0.2% it is slightly above it. This degradation in the energy resolution cannot be, however, compensated by an increase in the reduced electric field intensity. Based on both the approximate linear dependence of Q on the CO_2 concentration and the comparison with Magboltz simulations, these large fluctuations can be attributed to dissociative attachment of ionization electrons to CO_2 molecules. Seemingly, this process can only be mitigated by using shallower EL regions. Nevertheless, a compromise has to be found between the thickness of this region and the amount of EL produced.

The above findings are important for xenon-based TPCs relying on EL signal amplification, which are being increasingly used for rare-event detection such as directional dark matter, double electron capture and double beta decay detection. Particularly, the addition of CO_2 to pure xenon at the level of 0.05%–0.1% will reduce significantly the electron transverse diffusion from 10 $\text{mm}/\sqrt{\text{m}}$ to the level of few $\text{mm}/\sqrt{\text{m}}$, having a high impact on the discrimination of events through pattern recognition of the topology of primary ionization trails.

Other molecular additives, such as CH_4, do not present the drawback of having significant electron attachment but, on the other hand, higher concentrations will be needed to obtain similar electron transverse and longitudinal diffusions as in CO_2. Nevertheless, former work in [27] has shown that the addition of CH_4 to pure argon has less impact on the reduction in the mixture EL yield when compared to the addition of CO_2.

Acknowledgements

The NEXT Collaboration acknowledges support from the following agencies and institutions: the European Research Council (ERC) under the Advanced Grant 339787-NEXT; the Ministerio de Economía y Competitividad of Spain under grants FIS2014-53371-C04 and the Severo Ochoa Program SEV-2014-0398; the GVA of Spain under grant PROMETEO/2016/120; the Portuguese FCT under project PTDC/FIS-NUC/2525/2014; the U.S. De-

partment of Energy under contracts number DE-AC02-07CH11359 (Fermi National Accelerator Laboratory) and DE-FG02-13ER42020 (Texas A&M); the University of Texas at Arlington. C.A.O.H., E.D.C.F., C.M.B.M. and C.D.R.A. acknowledge FCT under grants PD/BD/105921/2014, SFRH/BPD/109180/2015, SFRH/BPD/76842/2011 and SFRH/BPD/79163/2011, respectively.

References

[1] J. Martin-Albo, et al., NEXT Collaboration, J. High Energy Phys. 5 (2016) 159.
[2] T. Brunner, et al., Int. J. Mass Spectrom. 379 (2015) 110.
[3] J. Galan, J. Instrum. 11 (2016) P04024.
[4] D.Yu. Akimov, et al., arXiv:physics/9704021v1, 16 Apr. 1997.
[5] Yu.M. Gavrilyuk, et al., Phys. At. Nucl. 78 (2016) 1563.
[6] D. Nygren, J. Phys. Conf. Ser. 460 (2013) 012006.
[7] G. Mohlabeng, et al., J. High Energy Phys. 7 (2015) 092.
[8] E. Aprile, et al., XENON100 Collaboration, Phys. Rev. Lett. 109 (2012) 181301.
[9] D.S. Akerib, et al., LUX Collaboration, Phys. Rev. Lett. 112 (2014) 091303.
[10] Andi Tan, et al., PandaX-II Collaboration, Phys. Rev. Lett. 117 (2016) 121303.
[11] J.B. Albert, et al., EXO-200 Collaboration, Nature 510 (7504) (2014) 229.
[12] A. Gando, et al., KamLAND-Zen Collaboration, Phys. Rev. Lett. 117 (2016) 082503.
[13] K. Abe, et al., XMASS Collaboration, Phys. Lett. B 759 (2016) 64.
[14] E. Aprile, et al., XENON Collaboration, Phys. Rev. C 95 (2017) 024605.
[15] R. Luescher, et al., Phys. Lett. B 434 (1998) 407.
[16] P. Ferrario, et al., NEXT Collaboration, J. High Energy Phys. 1 (2016) 104.
[17] D. González-Díaz, et al., NEXT Collaboration, Nucl. Instrum. Methods 604 (2015) 8.
[18] D. Lorca, et al., NEXT Collaboration, J. Instrum. 9 (2014) P10007.
[19] C.M.B. Monteiro, et al., J. Instrum. 2 (2007) P05001 and references therein.
[20] C.M.B. Monteiro, et al., Phys. Lett. B 668 (2008) 167.
[21] E.D.C. Freitas, et al., Phys. Lett. B 684 (2010) 205.
[22] C.M.B. Monteiro, et al., Phys. Lett. B 677 (2009) 133.
[23] C.M.B. Monteiro, et al., Phys. Lett. B 714 (2012) 18.
[24] C. Balan, et al., J. Instrum. 6 (2011) P02006.
[25] J.M.F. dos Santos, et al., X-Ray Spectrom. 30 (2001) 373 and references therein.
[26] J. Renner, et al., NEXT Collaboration, J. Instrum. 12 (2017) T01004.
[27] T. Himi, et al., Nucl. Instrum. Methods 205 (1983) 591.
[28] F.P. Santos, et al., J. Phys. D, Appl. Phys. 27 (1994) 42.
[29] C.D.R. Azevedo, et al., J. Instrum. 11 (2016) C02007.
[30] P.C.P.S. Simões, et al., X-Ray Spectrom. 30 (2001) 342.
[31] P.C.P.S. Simões, et al., Nucl. Instrum. Methods A 505 (2003) 247.
[32] J.A.M. Lopes, et al., IEEE Trans. Nucl. Sci. 48 (2001) 312.
[33] C.M.B. Monteiro, et al., IEEE Trans. Nucl. Sci. 48 (2001) 1081.
[34] T.H.V.T. Dias, et al., J. Appl. Phys. 82 (1997) 2742.
[35] D.F. Anderson, et al., Nucl. Instrum. Methods 163 (1979) 125.
[36] T.Z. Kowalski, et al., Nucl. Instrum. Methods A 279 (1989) 567.
[37] S.J.C. do Carmo, et al., IEEE Trans. Nucl. Sci. 55 (2008) 2637.
[38] S. Biagi, Degrad, http://consult.cern.ch/writeup/magboltz/.
[39] C. Azevedo, D. Gonzalez-Diaz, S. Biagi, et al., FERMILAB-PUB-17-267-CD, arXiv:1705.09481 [physics.ins-det], 2017.
[40] J. Escada, et al., J. Instrum. 4 (2009) P11025.
[41] S. Biagi, Magboltz, http://consult.cern.ch/writeup/magboltz/.
[42] E. Ruiz-Choliz, et al., Nucl. Instrum. Methods A 799 (2015) 137.
[43] V. Álvarez, et al., NEXT Collaboration, J. Instrum. 8 (2013) P09011.